Plasmon polaritons of metallic nanowires for controlling submicron propagation of light

Jean-Claude Weeber and Alain Dereux
Laboratoire de Physique, Optique Submicronique, Université de Bourgogne, BP 47870, F-21078 Dijon, France

Christian Girard
CEMES, 29 rue Jeanne Marvig, BP 4347, F-31055 Toulouse Cedex 4, France

Joachim R. Krenn and Jean-Pierre Goudonnet
Laboratoire de Physique, Optique Submicronique, Université de Bourgogne, BP 47870, F-21078 Dijon, France
(Received 29 April 1999)

We use the Green dyadic technique to study the propagation of a local excitation along metallic nanowires of a subwavelength cross section. The metallic nanowires are elongated parallelepipeds deposited on a transparent substrate. A tightly focused plane wave illuminates one end of the nanowires. The localized surface-plasmon resonances of the nanowires propagate the local excitations over distances larger than the incident wavelength. The properties of the electromagnetic eigenmodes of the nanowires are analyzed in terms of the local density of states. [S0163-1829(99)02136-0]

I. INTRODUCTION

The interaction of light with small metallic particles has been an intensive field of research for a long time.[1] Small metallic particles sustain electromagnetic modes known as localized surface plasmons (LSP's) which account for most of their optical properties. Up to the last decade, experimental studies of LSP's were restricted to the analysis of far-field properties of large ensembles of particles. Recent improvements of the near-field optical microscopy techniques nowadays allow the observation of LSP's in the vicinity of individual particles.[2,3] Near-field experiments have already demonstrated the possibility of probing the optical near-field generated by surface plasmons and, associated with localized plasmons of nanoscopic particles, metallic particle LSP's are suggested to be relevant to various technologies such as micro-optics[4] and light guiding devices of subwavelength size.[5] Recently, Quinten *et al.* theoretically investigated electromagnetic energy transfer along chains of spherical silver clusters.[6] On the basis of a model in which a plane electromagnetic wave is scattered and absorbed by only the first particle of the chain, they found that dipole-dipole coupling between the particles can be optimized to propagate this local excitation over a distance of several hundred nanometers. Plasmon coupling between small gold particles aligned to form a long linear chain was recently observed using a photon scanning tunneling microscope.[7]

In this paper, we demonstrate electromagnetic energy transport through metallic nanowires deposited on a dielectric substrate. The nanowires are metallic elongated parallelepipeds. The two short axes of the finite-size wires are much smaller than the incident wavelength, while the long axis is larger than this wavelength. We determine the propagation conditions of a local excitation along the nanowires by computing the near-field distribution above the nanowire when one end is locally illuminated by a focused plane wave. Section II summarizes the Green dyadic method used to perform such near-field calculations. The mathematical description of the electromagnetic field associated with a linearly polarized focused plane wave are also given in this section. The resonance conditions of a nanowire with fixed geometrical dimensions are presented in Sec. III. Section IV brings to the fore the usefulness of the concept of the electromagnetic local density of states (LDOS) to identify localized plasmon resonance. Section V demonstrates how to use the guiding properties of nanowires to excite single metallic particles.

II. THEORETICAL BACKGROUND

Most methods modeling the scattering of light by resonant metallic particles have a limited range of validity. For example, the quasistatic treatment of the scattering is reliable only if the geometrical dimensions of the particles are much smaller than the incident wavelength.[1] If the dimensions of the particles are not negligible compared to the incident wavelength, Mie's theory can be applied, but only in the case of scattering by spherical particles or clusters of spherical particles.[8] In our case, we consider an elongated nanowire with a long axis that is larger than the incident wavelength. To compute the field scattered by such a system, we use a rigorous Maxwell equations solver which accounts for the phase retardation effects and for the rather low symmetry of the particle. Among several techniques well suited to solve Maxwell equations accurately, we choose the Green dyadic method (GDM), because it provides a direct link to the formulation of the electromagnetic LDOS which will be used below.

A. Green dyadic method

The technique has been already widely described phenomena involving dielectric objects[9–13] or metallic resonant cluster aggregates.[14] In this section, we just summarize the main steps of the computational procedure.

The situation we consider is shown in Fig. 1. A nanowire with a volume Ω and a dielectric function ε_2 is deposited on the interface that separates two semi-infinite dielectric media

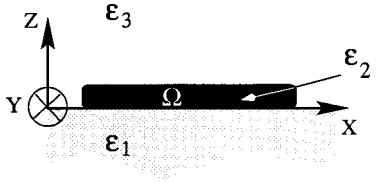

FIG. 1. Side view of the computational situation.

described by their dielectric constants ε_1 and ε_3. The system is illuminated by an incident beam, with an arbitrary space distribution and a harmonic time dependence of the form $\exp(-i\omega t)$. The electric field satisfies the vector wave equation

$$-\vec{\nabla}\times\vec{\nabla}\times\vec{E}(\vec{r},\omega)+\varepsilon(\vec{r},\omega)\frac{\omega^2}{c^2}\vec{E}(\vec{r},\omega)=0, \tag{1}$$

where $\vec{r}=(x,y,z)$ is the vector position and where the function $\varepsilon(\vec{r},\omega)$ is defined as

$$\varepsilon(\vec{r},\omega)=\varepsilon_2 \quad \text{if } \vec{r}\in\Omega,$$

$$\varepsilon(\vec{r},\omega)=\varepsilon_{ref}(z) \quad \text{if } \vec{r}\notin\Omega. \tag{2}$$

The dielectric function $\varepsilon_{ref}(z)$ that described the reference system, i.e., the flat interface separating the substrate ε_1 and the external medium ε_3, can be expressed as

$$\varepsilon_{ref}(z)=\varepsilon_3+\Theta(-z)(\varepsilon_1-\varepsilon_3), \tag{3}$$

where $\Theta(z)$ denotes the Heaviside function. Using this definition, Eq. (1) can be rewritten as

$$-\vec{\nabla}\times\vec{\nabla}\times\vec{E}(\vec{r},\omega)+\varepsilon_{ref}(z)\frac{\omega^2}{c^2}\vec{E}(\vec{r},\omega)$$

$$=\frac{\omega^2}{c^2}[\varepsilon_{ref}(z)-\varepsilon(\vec{r},\omega)]\vec{E}(\vec{r},\omega). \tag{4}$$

If the right-hand side of Eq. (4) is interpreted as a source term, the general solution of Eq. (4) can be expressed as a the sum of the incident field $\vec{E}_0(\vec{r},\omega)$ and the field $\vec{E}_s(\vec{r},\omega)$ scattered by the nanowire:

$$\vec{E}(\vec{r},\omega)=\vec{E}_0(\vec{r},\omega)+\vec{E}_s(\vec{r},\omega). \tag{5}$$

The field $\vec{E}_0(\vec{r},\omega)$ is the solution of Eq. (4) when its right-hand side is zero. It thus corresponds to the field refracted by the flat interface.

In order to determine $\vec{E}_s(\vec{r},\omega)$, one has to consider the Green dyadic $\overleftrightarrow{G}_{ref}(\vec{r},\vec{r}',\omega)$ associated with the bare interface, which is defined by

$$-\vec{\nabla}\times\vec{\nabla}\times\overleftrightarrow{G}_{ref}(\vec{r},\vec{r}',\omega)+\varepsilon_{ref}(z)\frac{\omega^2}{c^2}\overleftrightarrow{G}_{ref}(\vec{r},\vec{r}',\omega)$$

$$=\overleftrightarrow{\mathbf{1}}\delta(\vec{r}-\vec{r}'). \tag{6}$$

Taking the posterior scalar product of both sides of Eq. (6) with the vector $(\omega^2/c^2)[\varepsilon_{ref}(z)-\varepsilon(\vec{r},\omega)]\vec{E}(\vec{r},\omega)$, and integrating over the whole space with respect to $\vec{r}'$, leads to

$$\vec{E}_s(\vec{r},\omega)=\frac{\omega^2}{c^2}\int_\Omega d\vec{r}'\,\overleftrightarrow{G}_{ref}(\vec{r},\vec{r}',\omega)$$

$$\times[\varepsilon_{ref}(z_s)-\varepsilon(\vec{r}',\omega)]\vec{E}(\vec{r}',\omega). \tag{7}$$

Introducing Eq. (7) into Eq. (5), one obtains an implicit Lippmann-Schwinger equation

$$\vec{E}(\vec{r},\omega)=\vec{E}_0(\vec{r},\omega)+\frac{\omega^2}{c^2}\int_\Omega d\vec{r}'\,\overleftrightarrow{G}_{ref}(\vec{r},\vec{r}',\omega)$$

$$\times[\varepsilon_{ref}(z_s)-\varepsilon(\vec{r}',\omega)]\vec{E}(\vec{r}',\omega). \tag{8}$$

This Lippman-Schwinger equation (LSE) allows the calculation of the electric field anywhere in the space if the field inside the scatterer is known. However, the Green dyadic has to be derived first.

The tensor $\overleftrightarrow{G}_{ref}(\vec{r},\vec{r}',\omega)$ describes the electric field at the observation point $\vec{r}$ induced by a point source located at $\vec{r}'$. In our situation, each point inside the volume Ω of the wire is a point source. Since we are interested in the field scattered in the upper medium, the field emitted at $\vec{r}'$ can reach $\vec{r}$ after a direct propagation through the homogeneous upper medium or after reflection on the interface. As a consequence, the Green dyadic is expressed as a sum of two contributions,

$$\overleftrightarrow{G}_{ref}(\vec{r},\vec{r}',\omega)=\overleftrightarrow{G}_h(\vec{r},\vec{r}',\omega)+\overleftrightarrow{G}_{surf}(\vec{r},\vec{r}',\omega), \tag{9}$$

where $\overleftrightarrow{G}_h$ is the tensor associated with a homogeneous medium with a dielectric constant equal to ε_3, and where $\overleftrightarrow{G}_{surf}$ accounts for the interaction of the field radiated by the point source with the interface. The detailed calculation procedure of each contribution $\overleftrightarrow{G}_h$ and $\overleftrightarrow{G}_{surf}$ can be found respectively in Refs. 15 and 16.

To compute the field inside the particle numerically, it is first necessary to discretize the scatterer as an arrangement of N cells. If $\vec{r}_i$ denotes the center position of the ith cell, the LSE reduces to a linear system that can be written in the matrix form

$$\begin{pmatrix}\vec{E}(\vec{r}_1,\omega)\\ \vdots\\ \vec{E}(\vec{r}_N,\omega)\end{pmatrix}=\begin{pmatrix}\overleftrightarrow{1}-V\overleftrightarrow{G}_{ref}(\vec{r}_1,\vec{r}_1) & \cdots & V\overleftrightarrow{G}_{ref}(\vec{r}_1,\vec{r}_N)\\ \vdots & & \vdots\\ V\overleftrightarrow{G}_{ref}(\vec{r}_N,\vec{r}_1) & \cdots & \overleftrightarrow{1}-V\overleftrightarrow{G}_{ref}(\vec{r}_N,\vec{r}_N)\end{pmatrix}^{-1}\begin{pmatrix}\vec{E}_0(\vec{r}_1,\omega)\\ \vdots\\ \vec{E}_0(\vec{r}_N,\omega)\end{pmatrix}, \tag{10}$$

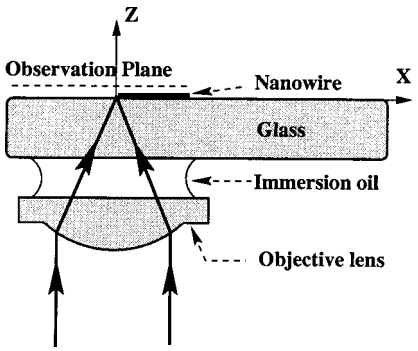

FIG. 2. Diagrammatic view of the local illumination of the nanowire by a focused plane wave.

where $V=(\omega^2/c^2)(\varepsilon_3-\varepsilon_2)v$, v being the volume of one cell. Since all the components of the electric field in the particles have been obtained from system (10), it is then a simple matter to derive the electric field anywhere in the upper medium using a discretized form of Eq. (8):

$$\vec{E}(\vec{r},\omega)=\vec{E}_0(\vec{r},\omega)+V\sum_{\vec{r}_i\in\Omega}\vec{\vec{G}}_{ref}(\vec{r},\vec{r}_i)\vec{E}(\vec{r}_i,\omega). \quad (11)$$

B. Focused plane-wave model

Near-field experiments demonstrating the local excitation of surface plasmons on thin films or LSP's on single metallic particles have already been reported.[17,18] The local excitation has been achieved by illumination through a tapered metal coated optical fiber which is equivalent to a subwavelength aperture. In our case, the local excitation of the nanowire is realized in a classical way with a focused plane wave. Let us consider the situation depicted in Fig. 2. A nanowire deposited on a glass plate is locally excited by a converging incident wave. The incident plane wave is focused through the glass plate by an immersion oil objective. The optical refractive index of the objective lens, the immersion oil, and the glass plate are chosen to be equal. If the optical index of the lens is only slightly different from the index of the surrounding medium, the application of the first Born approximation leads to neglect of the back-reflection of the scattered light on the entrance side of the objective lens. As a consequence, we can consider that the nanowire lies on a semi-infinite homogeneous medium. The field diffracted by the particle can thus be calculated using the GDM with the surface tensor defined above.

From Eqs. (10) and (11), all we need to compute the scattered field is the zero-order solution $\vec{E}_0(\vec{r},\omega)$, i.e., the electric field associated with the focused plane wave transmitted through the bare interface. Most of the works dealing with the scattering of finite-size beam rely on a plane-wave expansion of the beam in order to compute the contribution of each plane wave of the spectrum separately.[19,20] Because the GDM leads to a real-space discretization of the scatterer, such a procedure is not necessary in our case. We just need to know the components of the focused field $\vec{E}_0(\vec{r},\omega)$ at any point located in the upper medium $(z>0)$.

The model we use to describe the field $\vec{E}_0(\vec{r},\omega)$ was developed by Török and co-workers to study the structure of the electric field associated with a plane wave focused through an interface between two materials with different refractive indexes.[21–23] Assuming that the incident plane wave is linearly polarized along the x direction and is focused on the upper side of the interface, the electric field transmitted to the upper medium ε_3 reads

$$E_{0,x}(x,y,z)=-i\left[I_0+I_2\frac{(x^2-y^2)}{r_\parallel^2}\right],$$

$$E_{0,y}(x,y,z)=-iI_2\frac{2xy}{r_\parallel^2}, \quad (12)$$

$$E_{0,z}(x,y,z)=-2I_1\frac{x}{r_\parallel},$$

where $r_\parallel=(x^2+y^2)^{1/2}$, and where I_0, I_1, and I_2 are defined as follows:

$$I_0=\int_0^\alpha d\phi_1\sqrt{\cos\phi_1}\sin\phi_1(\tau_s+\tau_p\cos\phi_3)J_0(\sqrt{\varepsilon_1}k_0r_\parallel)\times\exp(i\sqrt{\varepsilon_3}k_0\cos\phi_3 z),$$

$$I_1=\int_0^\alpha d\phi_1\sqrt{\cos\phi_1}\sin\phi_1(\tau_p\sin\phi_3)J_1(\sqrt{\varepsilon_1}k_0r_\parallel)\times\exp(i\sqrt{\varepsilon_3}k_0\cos\phi_3 z),$$

$$I_2=\int_0^\alpha d\phi_1\sqrt{\cos\phi_1}\sin\phi_1(\tau_s-\tau_p\cos\phi_3)\times J_2(\sqrt{\varepsilon_1}k_0r_\parallel)\exp(i\sqrt{\varepsilon_3}k_0\cos\phi_3 z). \quad (13)$$

In Eqs. (13), α denotes the angle between the marginal rays and the z axis; τ_s and τ_p are the Fresnel coefficients for s and p polarized plane waves, respectively, and k_0 is the wave number of the incident wave in vacuum. The quantities J_0, J_1, and J_2 are the zeroth-, first-, and second-order Bessel functions of the first kind, respectively. The angles ϕ_1 and ϕ_3 are related by Snell's law. In order to show the structure of the focused electric-field wave, in Fig. 3 we report a sequence of electric intensity maps computed over the bare interface for an incident wavelength in vacuum $\lambda=633$ nm. The observation plane is in air $(\varepsilon_3=1.0)$ and is located at $z_{obs}=25$ nm over the glass substrate. The numerical aperture (NA) of the immersion objective lens has been chosen equal to 0.9. Such a value of the NA is realistic, and can be easily achieved with oil immersion microscope objectives. If the dielectric function of the glass substrate is $\varepsilon_1=2.25$, from the well-known relation $\alpha=\arcsin(\mathrm{NA}/\sqrt{\varepsilon_1})$, we find that the angle of incidence α of the marginal rays is about 36.9°. We have used 201 samples to perform the angular integration of I_0, I_1, and I_2. The four maps in Fig. 3 are normalized with respect to the electrical intensity at the intersection between the vertical axis passing over the focal point and the observation plane. The $|E^2|$ map shows a spot slightly elongated in the x direction. This nonsymmetric spot is mostly due to the contribution of the longitudinal z component of the electric field. The maximum contribution of the x, y, and

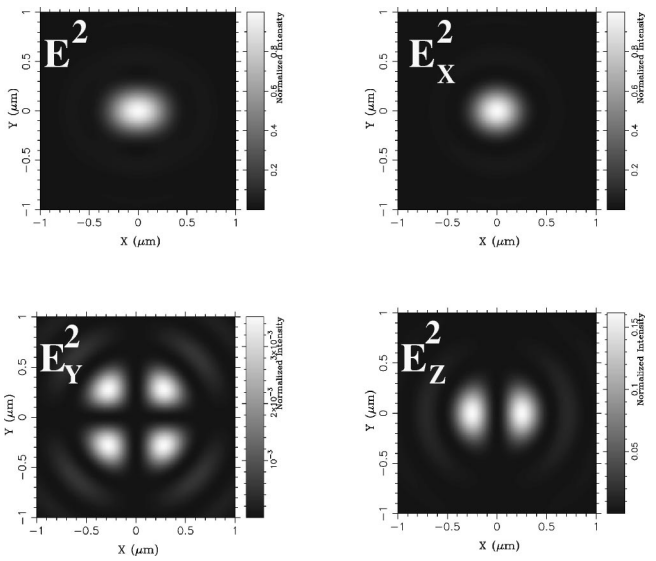

FIG. 3. Electric intensity maps of the focused plane wave transmitted through the bare glass-air interface. The incident plane wave is linearly *x* polarized, and the objective lens has a NA of 0.9.

z components to the total electric intensity are in the ratio of 1, 0.0035, and 0.16, respectively. The spatial distributions and the relative weights of each component can be directly compared to the results presented in Refs. 24–26. Except for the wavelength, the illumination conditions (polarization and NA of the objective) described above will be kept constant for all the numerical applications performed in the following sections.

III. NEAR-FIELD AROUND A RESONANT NANOWIRE

In this section, the propagation conditions of a local electromagnetic excitation along a metallic nanowire are determined. We first consider a nanowire made of gold with a length of 1.5 μm, a width of 30 nm, and a height of 15 nm. The dimensions of the nanowire have been chosen to be in the range of feasibility of current nanofabrication techniques such as electron-beam lithography.[27]

The optical properties of small metallic particles are strongly influenced by localized surface plasmon which are the collective oscillations of electrons. The LSP excitation conditions of nanoscopic metallic clusters are well understood on the basis of a relatively simple formula deduced within the nonretarded approximation (the quasistatic regime). In the case of nanowires, the elongation in one direction up to a mesoscopic size makes the matter more difficult because the phase retardation effects cannot be neglected anymore. Simple formulas similar to those produced by the nonretarded approximation are not available. Therefore, to determine the excitation conditions of nanowires, we numerically perform a spectroscopic analysis over a wide spectral range.

Figure 4 shows the spectrum of the intensity computed over the ''exit'' end of the nanowire when the incident wavelength is swept from the visible to the near-infrared. To compute this spectrum, the center of the incident beam has been shifted away from the other ''entrance'' end of the wire in order to reduce the area of the particle illuminated by the

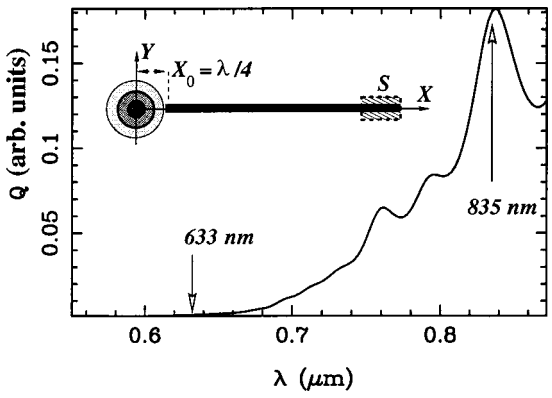

FIG. 4. Near-field spectra of the 1.5-μm-long nanowire. The incident spot center is shifted by a distance of $\lambda/4$ with respect to the ''entrance'' end of the nanowire. The detection area *S* is located 10 nm over the top of the nanowire.

incident light. The shift has been chosen to be λ dependent, and fixed to $\lambda/4$ in order to compensate for the spot size growing with increasing wavelength. In the numerical work, the scatterer is discretized with 1600 cubic cells. Because the volume of the wire is large enough to exclude intrinsic size effects, we use the bulk values tabulated by Palik to describe the dielectric function of gold.[28] The signal *Q* computed versus the wavelength is defined as

$$Q(\lambda)=\frac{1}{S}\int_s \frac{|E(x,y,z_{\rm obs},\lambda)|^2}{|E_0(x_b,y_b,z_{\rm obs},\lambda)|^2}\,dS, \qquad (14)$$

where *S* is an area with a surface of 100×50 nm^2 located above the ''exit'' end of the nanowire at a distance of 10 nm from the top of the nanowire. $E_0(x_b,y_b,z_{\rm obs},\lambda)$ is the electric field associated with the incident beam at the point located in the observation plane above the ''entrance'' of the wire. λ refers to the wavelength of the incident light in vacuum. The quantity $Q(\lambda)$ can be understood as a kind of near-field scattering coefficient[29] that measures the near-field response at the ''exit'' end of the wire relative to a given local excitation at the ''entrance.'' Eventually, this coefficient is proportional to the signal that would be detected by a photon scanning tunneling microscope. The spectrum plotted in Fig. 4 exhibits several peaks in the red and near-infrared regions. Because the peaks occur at low frequency, we can assume that they are related to longitudinal eigenmodes, i.e., excitation with the electric field parallel to the long axis *x* of the nanowire.[31,1] This assumption is supported by the fact that no significant signal is detected at the ''exit'' end of the wire if the incident beam is mostly polarized in the transverse *y* direction. Note that for microwave wavelengths, it is known that longitudinal resonances can be sustained by a highly conducting wire in free space when the wire's length is equal to an odd number of half-wavelengths.[30] Of course, in our situation, the high conductivity criterion is not verified for all wavelengths of the spectrum, so that the effect discussed here relies on the features of the frequency-dependent dielectric function of gold.

Figure 5 shows the spatial distribution of the near-field electric intensity over the wire for two incident wavelengths $\lambda=633$ and 835 nm. Similarly to the computed spectrum of Fig. 4, the observation plane is located 10 nm over the top of the wire and the intensity is normalized with respect to

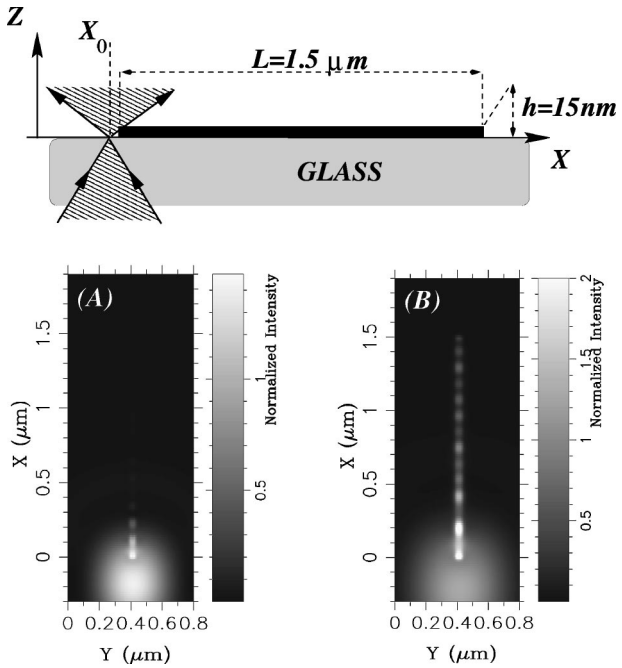

FIG. 5. Side view of the illumination condition and electric near-field map computed 10 nm over the top of the nanowire. (A) out of resonance, $\lambda = 633$ nm. (B) At resonance, $\lambda = 835$ nm.

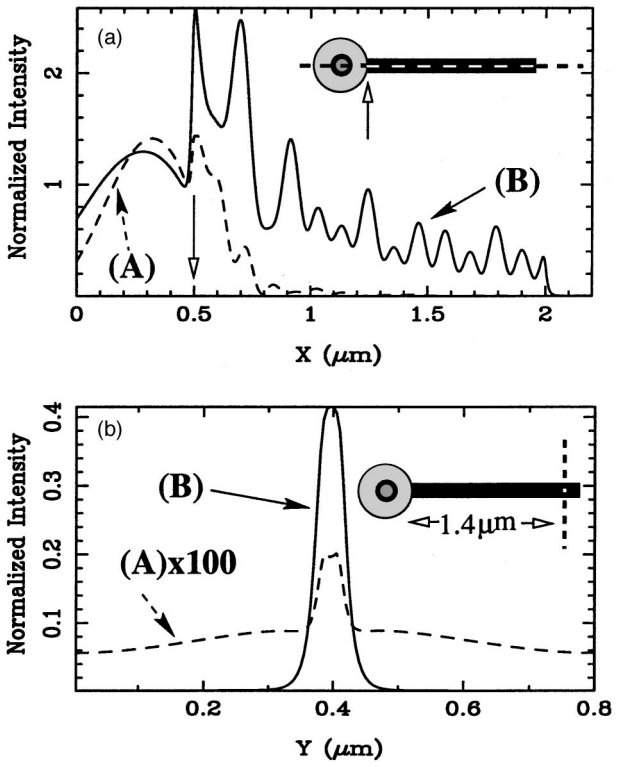

FIG. 6. Crosscuts of the near-field map shown in Fig. 5. (a) Along the x direction: (A) $\lambda = 633$ nm, and (B) $\lambda = 835$ nm. The white arrow shows the position of the ''entrance'' end of the nanowire. (b) Along the y direction: (A) $\lambda = 633$ nm [the initial values of (A) multiplied by 100], and (B) $\lambda = 835$ nm.

$|E_0(x_b, y_b, z_{\text{obs}}, \omega)|^2$. Out of resonance, for $\lambda = 633$ nm, only the area of the wire directly illuminated by the incident spot shows up in the near-field map. If λ is changed to 835 nm, we observe a kind of standing-wave pattern over the wire. To refine the analysis, in Fig. 6 we show a crosscut of both images in the x and y directions. For $\lambda = 633$ nm, the crosscut shows that the intensity along the x direction is strongly damped. For a distance of 250 nm from the ''entrance'' of the nanowire, the detected intensity is reduced to 10% of the normalized intensity. For $\lambda = 835$ nm, the normalized intensity exhibits a strongly oscillating behavior. The normalized intensity 1.4 μm away from the ''entrance'' end of the wire is still 40%. If the local probe of a near-field optical microscope is brought very close to the ''exit'' end of the wire, it should be possible to detect the field intensity of the LSP that has been excited by the incident beam. In that sense, the nanowire can be regarded as a subwavelength waveguide. Although the purpose of this work is not to optimize the waveguide performances of the nanowire, we can expect that the coupling efficiency with the eigenmode of the wire could be significantly improved by adjusting the parameters of dimensions and material of the wire. Such an optimization was shown to be possible by Quinten and Kreibig in the case of silver particles chains.[6] In order to gain more insight into the structure of the wire's eigenmodes, we introduce the concept of electromagnetic local density of state in Sec. IV.

IV. LOCAL DENSITY OF STATES ABOVE A METALLIC NANOWIRE

Up to now, we have used the GDM only to compute the electric near-field scattered by the nanowire, but much more physical information is contained in the Green dyadic. In analogy with the scalar Green's-function theory,[32,33] one can see that the LDOS can be extracted from the Green dyadic using the relation[34]

$$\eta(\vec{r},\omega) = -\frac{1}{\pi}\mathrm{Tr},\Im\,\overleftrightarrow{G}(\vec{r},\vec{r},\omega), \tag{15}$$

where Tr and $\Im$ stand for the trace and the imaginary part of $\overleftrightarrow{G}(\vec{r},\vec{r},\omega)$, respectively. In Eq. (15), the tensor $\overleftrightarrow{G}$ denotes the Green dyadic of the complete system, i.e., the reference system in the presence of scatterer. The calculation of $\overleftrightarrow{G}(\vec{r},\vec{r}',\omega)$ is performed thanks to the Dyson equation[15]

$$\overleftrightarrow{G}(\vec{r},\vec{r}',\omega) = \overleftrightarrow{G}_{ref}(\vec{r},\vec{r}',\omega) + \int_{\Omega} d\vec{r}''\,\overleftrightarrow{G}_{ref}(\vec{r},\vec{r}'',\omega)\,\overleftrightarrow{V}(\vec{r}'',\omega)\,\overleftrightarrow{G}(\vec{r}'',\vec{r}',\omega). \tag{16}$$

In the context of electron physics, the LDOS is understood as the density of the probability to find an electron at the observation point with a given energy. The density of the probability is related to the square modulus of the electron wave function which can be computed using the Green's-function formalism. In our case, the quantity we compute with the Green dyadic is the electric field. As a consequence, in analogy with the Green's-function theory, the electromagnetic LDOS calculated using Eq. (15) gives the square modulus of the electric field associated with the eigenmode of the scatterer at a given frequency. Note that the electromagnetic LDOS computed here does not correspond to the square

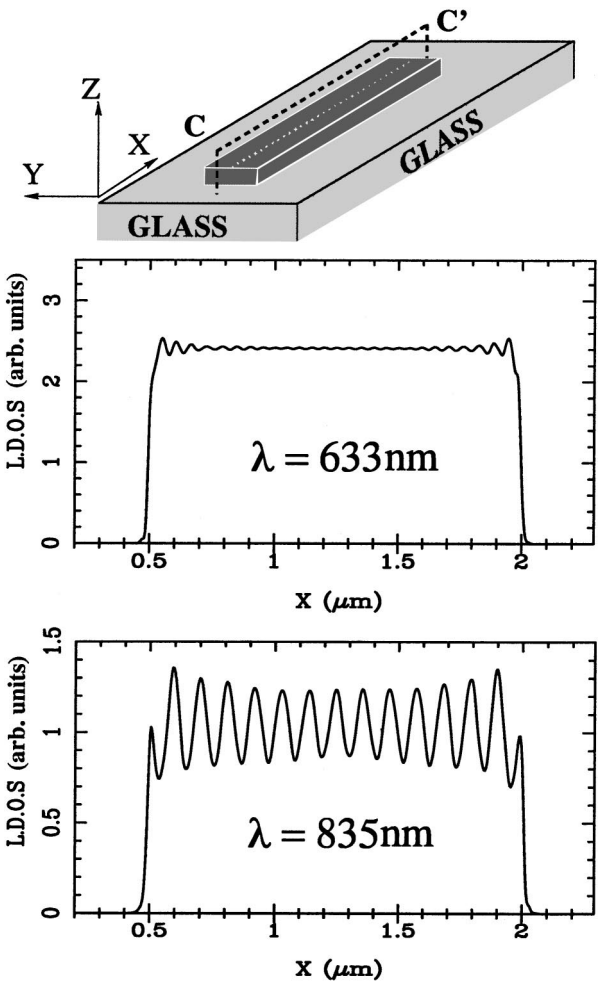

FIG. 7. Three-dimensional view of the computational situation. Electromagnetic LDOS profiles calculated along the line (C-C'). The line (C-C') is located 10 nm over the top of the wire.

modulus of a photon wave function since, in quantum field theory, the electric field is an observable and not a photon wave function.

In Fig. 7 we show the LDOS computed along the x direction, 10 nm over the top of the wire. The LDOS gives an image of the electric-field intensity associated with the eigenmodes of the object. The eigenmodes of the wires can be understood as solutions of the vector wave equation when no incident field illuminates the object. As a consequence, the LDOS profiles exhibit symmetric shapes, since no distorsion is induced by the superposition of the incident field. For a frequency that corresponds to $\lambda = 633$ nm, the LDOS shows an almost flat profile above the nanowire, except over the edges where tiny damped oscillations occur. Conversely, for $\lambda = 835$ nm, the LDOS profile exhibits a strong oscillating behavior. Except for the two sharp oscillations over the edges of the wire, we observe the same number of periods on the LDOS profile and on the corresponding crosscut of the normalized intensity reported in Fig. 6. It appears that the oscillations observed on the x crosscuts of Fig. 6 reveal the intrinsic structure of the excited eigenmode. Note that such a similarity between the LDOS and the electric intensity profiles is only observed when the incident light locally excites the nanowire. If the object is entirely excited by an incident plane wave, for example, polarization and phase effects may

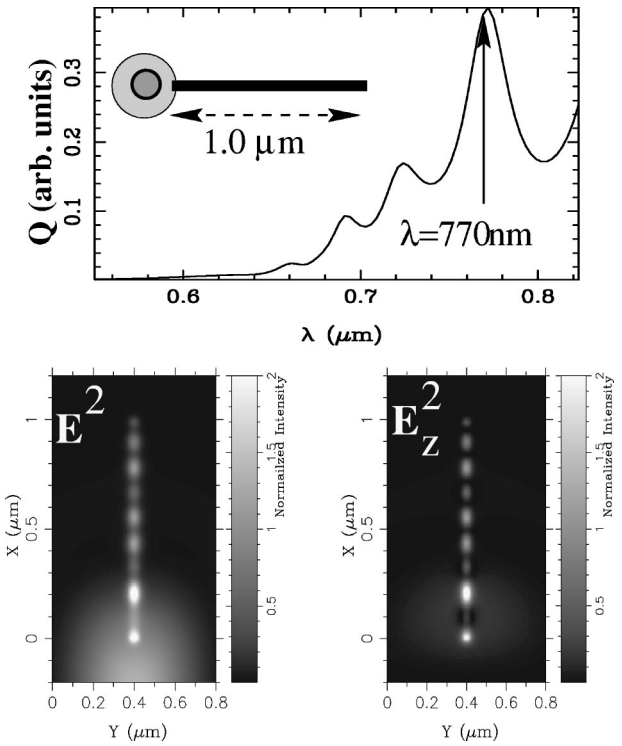

FIG. 8. Near-field spectrum of the 1.0-μm-long nanowire and electrical intensity near-field maps for $\lambda = 770$ nm. The observation plane is located 20 nm over the top of the object.

downgrade the agreement between the LDOS and the electric intensity. The physical explanation of such a result is contained in Eq. (11). Considering this equation, one can see that the total scattered field is the superposition of the incident field and the field radiated by the object. In the case of local illumination, because the amplitude of the incident field decays as a function of the distance to the focal point, we unambiguously observe the field associated with the eigenmode of the ''exit'' end of the nanowire. Conversely, if the nanowire is excited by a plane wave, the scattered field at any point above the object is a coherent sum of incident and radiated field that can mask the field of the nanowire eigenmode. We can conclude that an eigenmode of the wire is convenient to propagate a local excitation if the LDOS oscillates strongly over the object.

V. SINGLE-PARTICLE EXCITATION WITH A NANOWIRE WAVEGUIDE

In previous numerical applications, we have been interested in the total electric-field intensity. The GDM also offers the opportunity to investigate the contribution of each component of the electric field separately. Let us now consider a gold wire with a volume of $1000 \times 30 \times 20$ nm^3. The spectrum of the wire shown in Fig. 8 is obtained when the entrance of the nanowire is excited as in the previous case. The spectrum shows three neat resonance peaks in the visible range. We choose an incident wavelength of $\lambda = 770$ nm, and compute the near-field intensity in an observation plane located 20 nm over the top of the object. The $|E|^2$ and $|E_z|^2$ maps reported in Fig. 8 are plotted with the same gray scales. It appears that the z component of the electric field supports

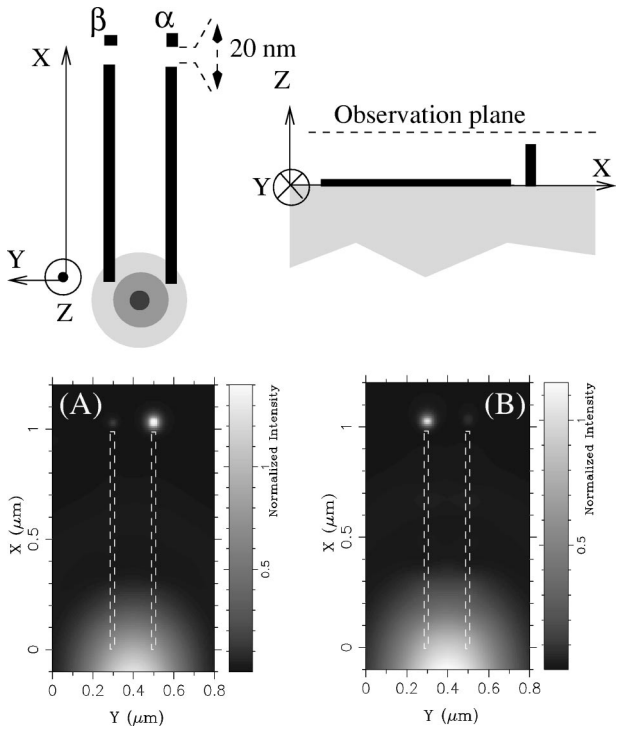

FIG. 9. Top and side views of the single particle excitation setup and near-field maps calculated 20 nm over the top side of the isolated particles. (A) $\lambda = 730$ nm. (B) $\lambda = 820$ nm. The dashed profiles show the position of the two nanowires used as waveguides.

most of the intensity detected over the nanowire. At the ''exit'' end of the wire, more than 90% of the total intensity is due to the *z* component. Note that this behavior is not inconsistent with an excitation of the *x* axis of the wire. A small prolate ellipsoid excited at the resonance frequency of its long axis can also scatter an electric near-field locally strongly polarized along a direction perpendicular to the excited axis. This result suggests that the electric field of the electromagnetic mode supported by the wire could be used to excite the *z* axis of a metallic particle placed close to the end of the nanowire. In order to check this hypothesis, we consider the situation depicted in Fig. 9. At the end of two 1-μm-long nanowires, we have placed two gold particles elongated in the *z* direction. Both particles, denoted α and β in Fig. 9, have a height of 100 nm. The β particle has a rectangular section of 20×30 nm^2, while the section of the α particle is square with a surface of 30×30 nm^2. Using the GDM, we have found that the *z* axis resonances of the particles α and β occur at $\lambda_\alpha = 730$ nm and $\lambda_\beta = 820$ nm, respectively. Even if these two wavelengths do not correspond to maxima of resonance peaks of the 1-μm-long nanowire (cf. Fig. 8), the quantity Q has a significant value for both λ_α and λ_β. These two wavelengths have been used to compute the maps shown in Fig. 9. One can see that, depending on the wavelength, a bright spot appears above one or the other particle. Because the field amplitude of the nanowire mode is exponentially damped with the observation height, we cannot observe propagation along the wires. To reach the two particles, the field of the nanowire mode has tunneled across an air gap of 20 nm. In spite of the damping induced by the tunneling, the coupling between the wire and the particles remains efficient. Such a configuration could be of experimental interest for many applications, since it achieves a single-particle excitation with the opportunity to switch from one particle to another by adjusting the incident wavelength.

VI. CONCLUSION

Using a rigorous Maxwell's equation solver based on Green's dyadic technique, we have investigated the plasmon excitation of metallic nanowires. If the incident beam is polarized parallel to the long axis of the particle and illuminates one of the end of the nanowire, the local excitation can be guided along the nanowire by means of localized surface plasmon over distances larger than the incident wavelength. When locally excited at the resonance frequency, the electric near-field intensity scattered by the nanowire is related to the electromagnetic LDOS profiles computed over the object. Therefore, local illumination offers the opportunity to observe directly the structure of the eigenmodes sustained by the nanowires. Finally, we presented examples of the use of nanowires to excite individual particles at different wavelengths.

ACKNOWLEDGMENTS

The CEMES is UPR CNRS 8011. This work benefitted from the financial support of the Region of Burgundy. Additional support from the Austrian Fond zur Förderung der wissenschaftlichen Forschung, Grant No. P11476, and the Nationalbank Jubiläumsfond, Project No. 6256, is acknowledged.

[1] U. Kreibig and M. Vollmer, *Optical Properties of Metal Clusters*, Springer Series in Materials Science Vol. 25 (Springer, New York, 1993).

[2] J. R. Krenn, W. Gotschy, D. Somitsch, A. Leitner, and F. R. Aussenegg, Appl. Phys. A: Solids Surf. **61**, 545 (1995).

[3] I. I. Smolyaninov, D. L. Mazzoni, and C. C. Davis, Phys. Rev. Lett. **77**, 3877 (1996).

[4] S. I. Bozhevolnyi and F. A. Pudonin, Phys. Rev. Lett. **78**, 2823 (1997).

[5] J. Takahara, S. Yamagishi, H. Taki, A. Morimoto, and T. Kobayashi, Opt. Lett. **22**, 475 (1997).

[6] M. Quinten, A. Leitner, J. R. Krenn, and F. R. Aussenegg, Opt. Lett. **23**, 1331 (1998).

[7] J. R. Krenn, A. Dereux, J. C. Weeber, E. Bourillot, Y. Lacroute, J. P. Goudonnet, G. Schider, W. Gotschy, A. Leitner, F. R. Aussenegg, and C. Girard, Phys. Rev. Lett. **82**, 2590 (1999).

[8] M. Quinten and U. Kreibig, Surf. Sci. **172**, 557 (1986).

[9] Ch. Girard and A. Dereux, Rep. Prog. Phys. **59**, 657 (1996).

[10] Ch. Girard, A. Dereux, O. J. F. Martin, and M. Devel, Phys. Rev. B **50**, 14 467 (1994).

[11] O. J. F. Martin, Ch. Girard, and A. Dereux, J. Opt. Soc. Am. A **13**, 1801 (1996).

[12] Ch. Girard, J. C. Weeber, A. Dereux, O. J. F. Martin, and J. P. Goudonnet, Phys. Rev. B **55**, 16 487 (1997).
[13] J. J. Greffet and R. Carminati, in *Optics at the Nanometer Scale*, Vol. 319 of *NATO Advanced Study Institute, Series E: Applied Sciences*, edited by M. Nieto-Vesperinas (Kluwer, Dordrecht, 1996), pp. 1–26.
[14] Ch. Girard and A. Dereux, Phys. Rev. B **49**, 11 344 (1994).
[15] O. J. F. Martin, Ch. Girard, and A. Dereux, Phys. Rev. Lett. **74**, 526 (1995).
[16] N. Richard, A. Dereux, T. David, E. Bourillot, J. P. Goudonnet, F. Scheurer, E. Beaurepaire, and G. Garreau, Phys. Rev. B **59**, 5936 (1999).
[17] B. Hecht, H. Bielefeldt, L. Novotny, Y. Inouye, and D. W. Pohl, Phys. Rev. Lett. **77**, 1889 (1996).
[18] T. Klar, M. Perner, S. Grosse, G. von Plessen, W. Spirkl, and J. Feldmann, Phys. Rev. Lett. **80**, 4249 (1998).
[19] E. E. Kriezis, P. K. Pandelakis, and A. G. Papagiannakis, J. Opt. Soc. Am. A **11**, 630 (1994).
[20] E. E. M. Khaled, S. C. Hill, and P. W. Barber, IEEE Trans. Antennas Propag. **41**, 295 (1993).
[21] P. Török, P. Varga, Z. Laczik, and G. R. Booker, J. Opt. Soc. Am. A **12**, 325 (1995).
[22] P. Török, P. Varga, and G. R. Booker, J. Opt. Soc. Am. A **12**, 2136 (1995).
[23] P. Török, P. Varga, and G. R. Booker, J. Opt. Soc. Am. A **13**, 2232 (1996).
[24] M. Mansuripur, J. Opt. Soc. Am. A **3**, 2086 (1986).
[25] M. Mansuripur, L. Li, and W. Yeh, Opt. Photonics News **9**, 56 (1998).
[26] M. Mansuripur, L. Li, and W. Yeh, Opt. Photonics News **9**, 42 (1998).
[27] J. R. Krenn, R. Wolf, A. Leitner, and F. R. Aussenegg, Opt. Commun. **137**, 46 (1997).
[28] E. D. Palik, in *Handbook of Optical Constants of Solids*, edited by E. D. Palik (Academic Press, New York, 1985).
[29] B. J. Messinger, K. Ulrich von Raben, Richard K. Chang, and Peter W. Barber, Phys. Rev. B **24**, 649 (1981).
[30] P. C. Waterman and J. C. Pedersen, J. Opt. Soc. Am. A **15**, 174 (1998).
[31] C. G. Bohren and D. R. Huffman, in *Absorption and Scattering of Light by Small Particles*, edited by A. D. Boardman (Wiley, New York, 1983).
[32] E. N. Economou, *Green's Function in Quantum Physics* (Springer-Verlag, Berlin, 1983).
[33] A. Dereux, J. P. Vigneron, P. Lambin, and A. A. Lucas, Phys. Rev. B **38**, 5438 (1988).
[34] A. Dereux, Ph.D. thesis, University of Namur, Belgium, 1991.